HHS Public Access
Author manuscript
Acta Biomater. Author manuscript; available in PMC 2023 March 01.

Published in final edited form as:
Acta Biomater. 2022 March 01; 140: 338–349. doi:10.1016/j.actbio.2021.12.008.

Hybrid Nanocoatings of Self-assembled Organic-Inorganic Amphiphiles for Prevention of Implant Infections

Zhou Ye[1,#,*,†], **Ting Sang**[2,#], **Kun Li**[2], **Nicholas G. Fischer**[1], **Isha Mutreja**[1], **Constanza Echeverría**[3], **Dhiraj Kumar**[1], **Zhen Tang**[2,*], **Conrado Aparicio**[1,*,‡]

[1]MDRCBB, Minnesota Dental Research Center for Biomaterials and Biomechanics, University of Minnesota, Minneapolis, Minnesota 55455, United States

[2]The Affiliated Stomatological Hospital of Nanchang University & The Key Laboratory of Oral Biomedicine, Nanchang, Jiangxi Province 330006, China

[3]Cariology Unit, Department of Oral Rehabilitation, University of Talca, Talca 3460000, Chile

Abstract

Antimicrobial coatings are one of the most promising strategies to prevent bacterial infections in orthopedic and dental implants. Combining antimicrobial agents with different antimicrobial mechanisms might have synergistic effects and be more potent. Others have shown that nanocomposites of silver nanoparticles (AgNPs) decorated with antimicrobial peptides (AMPs) show increased potency as free agents in solution. However, similar nanocomposites have not been explored to coat biomaterials through cooperative weak electrostatic attraction forces between AMP, AgNPs and substrates in need of protection against infection. In this work, we synthesized self-assembled antimicrobial amphiphiles of an AMP, GL13K. Then, we decorated the AMP nanostructures with AgNPs, which were finally used to coat etched Ti (eTi) surfaces. The strong hydrogen bonding between the AMP amphiphiles and the polar eTi yielded a robust and stable coating. When compared to single AgNP or single AMP coatings, our hybrid nanocoatings had notably higher *in vitro* antimicrobial potency against multiple bacteria strains related to implant infection. The hybrid coating also showed relevant antimicrobial activity in an *in vivo* subcutaneous infection model in rats. This work advances the application of AgNP/AMP nanocomposites as effective coatings for prevention of implant infections.

Statement of significance—High morbidity, mortality and elevated costs are associated with orthopedic and dental implant infections. Conventional antibiotic treatment is ineffective due to

---

[*] Corresponding authors: Z. Y. zye2@nd.edu; Z. T. tangzhen307@aliyun.com; C. A. cjaparicio@uic.es.
[#] These authors contributed equally to this work
[†] Z.Y. current address: University of Notre Dame, Department of Chemical & Biomolecular Engineering, Notre Dame, Indiana 46556, United States
[‡] C.A. current address: UIC Barcelona – Universitat Internacional de Catalunya, Josep Trueta s/n, 08195 Sant Cugat\del Valles (Barcelona), Spain.

Declaration of competing interest
The authors declare that they have no known competing financial interests or personal relationships that could have appeared to influence the work reported in this paper.

Publisher's Disclaimer: This is a PDF file of an unedited manuscript that has been accepted for publication. As a service to our customers we are providing this early version of the manuscript. The manuscript will undergo copyediting, typesetting, and review of the resulting proof before it is published in its final form. Please note that during the production process errors may be discovered which could affect the content, and all legal disclaimers that apply to the journal pertain.

Author Manuscript
Author Manuscript
Author Manuscript
Author Manuscript

Author Manuscript Author Manuscript Author Manuscript Author Manuscript

barrier-like extracellular polysaccharide substances in biofilms and the increasing threat from antibiotic resistance. Antimicrobial coatings are one of the most promising strategies, but the performance is usually unsatisfactory, especially when tested *in vivo*. Here, we present a hybrid nanocoating with different modes of action to prevent implant infections using self-assembled antimicrobial peptide (AMP) amphiphiles decorated with silver nanoparticles (AgNPs). When compared to single AgNP or AMP coatings, our hybrid nanocoatings showed significant increases in antimicrobial potency against multiple implant infection-related bacterial strains *in vitro* and in an *in vivo* rat subcutaneous infection model.

Graphical Abstract

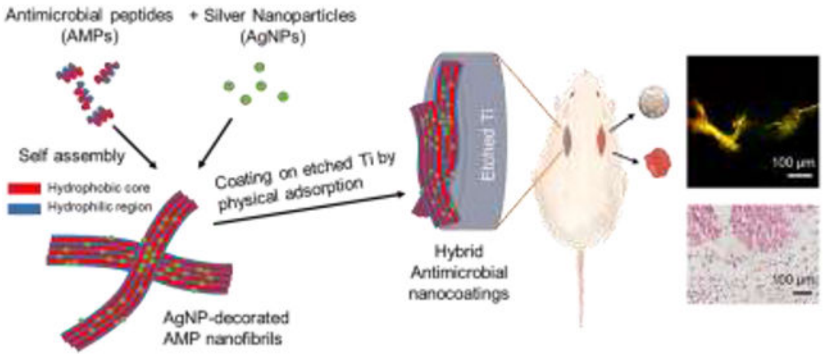

Keywords

antimicrobial coatings; hybrid nanostructures; antimicrobial peptides; silver nanoparticle; peri-implant infections

---

1. Introduction

Bacterial infection is one of the main causes for orthopedic and dental implant failures.[1-5] Resistogram-compliant antibiotic therapy is ineffective due to barrier-like extracellular polymeric substances in biofilms and the increasing threat from antibiotic resistance.[6] Surface modifications, including coatings on titanium (Ti) implants with antimicrobial agents have been demonstrated as one of the most effective strategies to prevent bacterial adhesion and/or kill colonized bacteria.[7-9] Different types of coatings have been extensively explored in previous studies, including metal ions and nanoparticles,[10-12] antibiotics,[13,14] antimicrobial peptides (AMPs),[15-17] and cationic polymers.[18,19] Three main antimicrobial mechanisms apply to these coatings: controlled release of antimicrobial agents, contact killing, and anti-adhesion/antifouling. Although these coatings showed great antimicrobial efficiency *in vitro*, most of their *in vivo* responses were inevitably inhibited due to the complex environment of implant associated infections, such as multi-strain biofilms and the degradation of antimicrobial agents.[7] Other concerns with current coating technologies include chemical and mechanical stability, scalability, and toxicity.[8]

Combinations of antimicrobial agents and/or methods for their application have not translated into a more effective antimicrobial coating in many cases. For example, the

Author Manuscript Author Manuscript Author Manuscript Author Manuscript

combination of chitosan and silver in a coating showed no better *in vivo* activity than the chitosan-only coating.[20] A more promising strategy is to combine antimicrobial agents and/or methods for their application with distinct killing mechanisms for synergistic effects, such as the combinations of antibiotic/silver nanoparticle (AgNP),[21] AMP/metal ion,[22] photodynamic therapy/AgNP,[23] or photodynamic/photothermal therapies.[24] These synergistic interactions can be based on antimicrobial agents with different bacterial targets and/or agents that could potentiate the activity of each other. Previous work applying multi-agent coatings focused on incorporating functionalities other than antimicrobial, such as osteogenesis,[25,26] angiogenesis,[27] or both,[28,29] but the antimicrobial activity itself was not improved compared to that obtained by applying single agent coatings.

AMP and AgNP nanocomposites have shown promising results as antimicrobial agents with enhanced efficacy in solution.[30-33] The potentiated antimicrobial efficacy mainly relied on the permeabilization of the bacterial membrane by AMPs to facilitate silver access to bacterial internal targets.[31] Previous AMP/AgNP combinations were based on the electrostatic attraction or covalent conjugation of single AMPs onto AgNP surfaces. Such AMP/AgNP combinations were exploited only as free antimicrobial agents and not coatings given that when AgNPs, which are negatively charged, are combined with AMPs, which are mostly positively charged, the AgNPs overall surface charge is notably neutralized, which in turn hinders electrostatic interactions with charged substrates.

To develop a stable and active coating we designed a hybrid nanocoating made of AgNPs decorating self-assembled AMP nanostructures (Scheme 1). GL13K, the AMP we used in this study, self-assembles in alkaline solution to form nanoribbons, a key structural feature for its antimicrobial activity and strong affinity to hydrophilic substrates.[34-36] GL13K coatings alone are stable and antimicrobial against both Gram-positive and Gram-negative pathogenic bacteria and biofilms on hydrophilic substrates, including titanium, mineralized collagen, dentinal tissue, and polysaccharide membranes.[37-41] Introducing negatively charged AgNPs onto positively charged AMP amphiphiles significantly reduces the electrostatic attraction between AMP amphiphiles and substrates. However, the self-assembled AMP/AgNP complexes in this work are expected to form stable coatings, as our previous work demonstrated that the dominant forces between AMP amphiphiles and polar substrates (e.g., Ti) were hydrophilic interactions via hydrogen bonding, but not strong electrostatic attraction.[35] This unique coating strategy circumvents previous challenges to coat AMP-decorated AgNPs, which mainly relied on the electrostatic interactions between AMP-decorated AgNPs and substrates. Our goal was to obtain a synergistic antimicrobial effect of AMPs and AgNPs in this nanocoating by combining short and long-distance antimicrobial effects, that is, killing of bacteria by direct contact with the surface-immobilized AMPs and potency by the released silver against bacteria in biofilms away from the implant surface.

2. Materials and methods

2.1. Materials

Silver nitrate, sodium citrate, sucrose, sodium tetraborate, and sodium hydroxide were purchased from MilliporeSigma (Burlington, MA, USA). GL13K (GKIIKLKASLKLL-

Author Manuscript Author Manuscript Author Manuscript Author Manuscript

NH_2) with molecular weight (MW) of 1424 g/mol and purity >98% was purchased from AAPPTec, LLC (Louisville, KY, USA). GL13K with all d-amino acids (dGL13K, Gkiiklkaslkll- NH_2) with purity >98% was purchased from Bankpeptide, Ltd (Hefei, Anhui, China). Commercially pure Titanium Grade II discs (Ø6 mm) were purchased from McMaster-Carr (Robbinsville, NJ, USA).

2.2. Fabrication of AgNPs

AgNPs were synthesized by the modified Turkevich method.[42] Briefly, 500 mL of 1 mM silver nitrate solution was heated to near boiling and kept at 93-94 °C in a water bath. Then, 10 mL of 250 mM sodium citrate solution was added dropwise to the silver nitrate solution with stirring. When the mixed solution turned grayish yellow, it indicated the formation of AgNPs. After 10 min, the solution was cooled down to room temperature (RT, 20-25 °C) and centrifuged at 35,280 RCF for 4×30 min to collect the highest amount possible of AgNPs in the pellet. The collected pellet was washed three times by carefully removing the supernatant, resuspending AgNPs in deionized (DI) water with resistivity of 18.2 MΩ·cm (Milli-Q system, MilliporeSigma, Burlington, MA, USA), and centrifuging at 2,380 RCF for 10 min. The final resuspended AgNP solution was diluted to OD_{420} of 2.9. Afterwards, 10 wt% sucrose was added to the AgNP solution as a cryo-protector and mixed by stirring for 2 h.[43] The AgNP-sucrose cake was obtained after lyophilization and weighted to calculate the weight percentage of AgNPs in the cake. The AgNP-sucrose cake was stored at −20 °C before use.

2.3. Preparation of nanocoatings

A stock solution of 100 mg/mL GL13K was prepared in DI water and vortexed to aid dissolution of all peptides. Borax-NaOH buffer at pH 9.8 was prepared by mixing a 0.025 M borax solution and a 0.1 M NaOH solution. The self-assembly of GL13K was triggered by adding 10 μL of the stock solution into 990 μL of the pH 9.8 borax-NaOH buffer to a final concentration of 1 mg/mL GL13K, either without AgNPs or with AgNPs to form the AgNP-GL13K complexes. The aforementioned solutions were stored at 4 °C or RT for 4 days to complete the peptide self-assembling before further characterizations or usage.

Ti discs were ground with 320-grit SiC disks (Buehler, Lake Bluff, IL, USA), polished with 9-μm MetaDi Supreme polycrystalline diamond suspension (Buehler, Lake Bluff, IL, USA) and 0.02-μm MasterMet 2 silica suspension (Buehler, Lake Bluff, IL, USA), etched by 5 M NaOH at 60 °C overnight, rinsed gently with DI water, dried with nitrogen, and immediately used to be coated. The etched Ti (eTi) discs were incubated in the AgNP solutions at 0.2 mg/mL, 1 mg/mL, and 5 mg/mL at RT overnight (12-18 h), referred to as 0.2Ag, 1Ag, and 5Ag, respectively. The estimated number of particles per total volume of solution were $3.9*10^{15}$, $2.0*10^{16}$, $9.8*10^{16}$ $mL^{-}1$, respectively (average particle diameter, from TEM analysis, of 2.1 nm, silver density of 10.5 g/cm^3). The eTi discs were incubated in the GL13K solution or the AgNP-GL13K solutions at 4 °C or RT overnight, referred to as GL/4C, 0.2Ag-GL/4C, 1Ag-GL/4C, and 5Ag-GL/4C for the ones at 4 °C and GL/RT, 0.2Ag-GL/RT, 1Ag-GL/RT, and 5Ag-GL/RT for the ones at RT. The groups coated with dGL13K or AgNP-dGL13K were referred to as dGL/4C or 0.2Ag-dGL/4C. The coated eTi

Author Manuscript Author Manuscript Author Manuscript Author Manuscript

discs were rinsed with DI water, dried with nitrogen, and stored in a vacuum desiccator for further experiments.

2.4. Materials characterizations

2.4.1 Transmission electron microscopy (TEM)—

Lyophilized AgNP-sucrose cake was dissolved in DI water to prepare a 1 mg/mL AgNP solution. A droplet of the AgNP solution was dispersed on a glass slide. A negatively charged copper grid with a carbon film was placed on the water-air interface and was kept floating on the surface for 10 min to collect AgNPs. TEM samples of GL13K were prepared by dispersing 3 μL of the GL13K solutions onto a negatively charged copper grid with a carbon film, followed by negative staining with 0.75% uranyl formate. The AgNP+GL13K complex was not stained. TEM was performed using a FEI Tecnai G2 F30 (Hillsboro, Oregon, USA) at an accelerating voltage of 300 kV.

2.4.2 Dynamic light scattering (DLS) and zeta potential measurement—

The AgNP solutions at a concentration of 0.2 mg/mL were prepared in DI water or the borax-NaOH buffer. Hydrodynamic diameter and zeta potential of AgNPs were measured by the Nanoflex 180° DLS system in a glass bottle and the Stabino particle charge titration analyzer using a PTFE chamber and a PTFE piston setup including a pH probe, respectively (Microtrac, Meerbusch, Germany). To perform the titration, the AgNP solution in borax-NaOH was first brought to pH 11 using a 0.1 N NaOH solution. Then it was followed by a system controlled addition of a 0.1 N HCl solution to complete the titration of zeta potential at the pH range of 11 to 2.

2.4.3 Circular Dichroism (CD)—

CD samples were prepared by adding 200 μL of the GL13K solutions into a quartz cuvette with a 1 mm path-length. CD spectra were monitored with a Jasco J-815 CD spectrometer (Easton, MD, USA) at RT. The CD signal was collected over a wavelength range of 190 nm to 260 nm with a data pitch of 1.0 nm, a scanning speed of 50 nm/min and a response time of 2 s. All measurements were corrected by subtracting the buffer spectrum and were obtained by the average of three scans. Estimations for secondary structure contents were obtained from further analysis of CD spectra using the BeStSel (Beta Structure Selection) method (http://bestsel.elte.hu/).[44]

2.4.4 Scanning electron microscopy (SEM)—

The morphology of etched titanium (eTi) was imaged with a field-emission SEM (Hitachi SU8230, Tokyo, Japan) at an accelerating voltage of 3 kV. The specimen was sputter-coated with a 5 nm-thick iridium layer.

2.4.5 X-ray photoelectron spectroscopy (XPS)—

A PHI 5000 Versa Probe III (ULVAC Inc, Kanagawa, Japan) XPS with a monochromatic Al Kα X-ray source (45°, 1486.6 eV, 50 W, sampling area: 200 μm diameter) was used to determine the elemental composition of the uncoated and coated eTi under ultra-high vacuum (10^{-8} Pa). All eTi discs were gently dried with a nitrogen stream and stored in a vacuum desiccator overnight before XPS analysis. Survey spectra were collected at 0-1100 eV using a pass energy of 280 eV with a step size of 1.0 eV. Three samples were scanned per group while each

Author Manuscript Author Manuscript Author Manuscript Author Manuscript

sample was measured in 4 different locations with 15 scans per location. Peak fitting and semi-quantification of surface elemental composition were performed in MultiPak (PHI, ULVAC Inc, Kanagawa, Japan).

2.4.6 Water contact angle (WCA) measurement—WCA measurement was used to evaluate the hydrophobicity of the sample surfaces coated with AgNP, GL13K, or AgNP-GL13K. The measurements were performed with the sessile drop method with a contact angle goniometer (DM-CE1, Kyowa Interface Science, Japan) and FAMAS software (Kyowa Interface Science, Japan). A 1.5 μL droplet of DI water was deposited on the tested surface with a tracking time of 60 s. Three samples were measured per group.

2.5. *In vitro* antimicrobial test

2.5.1 Bacterial culture—Antimicrobial activity was first evaluated against Streptococcus gordonii M5, a primary colonizer in oral biofilms. S. gordonii was inoculated on a brain heart infusion (BHI) agar plate in an aerobic incubator at 37 °C for 48 h. Afterwards, 3-5 colonies were picked and incubated in Todd-Hewitt broth (THB) in an aerobic incubator at 37 °C and 150 rpm until OD600 of 0.20. MRSA *and P. aeruginosa* (ATCC 27853) were isolated from patients by The First Affiliated Hospital of Nanchang University and inoculated on a blood agar plate in an aerobic incubator at 37°C for 24 h. Afterwards, 3-5 colonies of MRSA or *P. aeruginosa* were picked and incubated in 7.5% NaCl broth or BHI broth, respectively, in an aerobic incubator at 37°C and 150 rpm until OD_{600} of 0.20.

2.5.2 Antimicrobial test in quasi-static condition—Noncoated and coated eTi discs were sterilized by UV light for 20 min on each side and conditioned with 1 mL culturing medium at 37 °C for 30 min. The bacterial solutions (*S. gordonii*, MRSA, *or P. aeruginosa*) were diluted to OD_{600} of 0.02 (2×10^7, 2×10^6, 2×10^7 CFU/mL, respectively) in culture media (THB, 7.5% NaCl, and BHI, respectively) and added to each well to replace the medium. Samples were incubated at 37 °C and 150 rpm aerobically for 6 h. Two eTi discs were placed in medium without bacteria as a control. After 6 h incubation, samples were gently rinsed with 1× phosphate buffer saline (PBS) twice to remove the loosely attached bacteria before characterizations. Three independent experiments were conducted for each bacterial strain.

2.5.3 Antimicrobial test in a bioreactor—A drip flow bioreactor (Figure S4) was used as a model to simulate oral conditions. Four groups (eTi, 0.2Ag, GL/4C, and 0.2Ag-GL/4C) with 6 samples in each group were placed into four separate channels. All samples were first incubated in *S. gordonii* solution with OD_{600} of 0.02 for 6 h following the same method of static biofilm culturing. Afterwards, the samples were transferred into the bioreactor and continually cultured in medium (no bacteria) with a flow speed of 0.3 mL/min at 37 °C for 48 h. The bioreactor channels were put on a 10° inclined base to let the dripped medium flow over the samples.

2.5.4 ATP bioluminescence assay—Viable bacteria on samples after the 6 h incubation were quantified with the BacTiter-GloTM Microbial Cell Viability Assay

Author Manuscript

Author Manuscript

Author Manuscript

Author Manuscript

(Promega, Madison, WI, USA). After washed with 1×PBS, the samples were transferred to a new 48-well plate with an equal volume (200 μL) of the BacTiter-GloTM reagent and 1×PBS in each well. After incubating in dark for 5 min, 200 μL of the mixed solution was transferred into a black 96-well plate and measured with a microplate reader (BioTek, Winooski, VT, USA). Luminescence intensities were normalized to the average intensity of uncoated eTi samples in each experiment. Each experiment included four samples per group and was repeated in triplicate.

2.5.5 Colony forming units (CFU)—Bacteria on eTi surfaces were collected by cavitron ultrasonication for 90 s, followed by vortexing and sonication for 3×30 s each in ice bath. 100 μL of the collected bacterial solution was serially diluted by 10-10,000 folds. Then 100 μL of each dilution was plated on BHI agar plates and incubated aerobically at 37 °C for 48 h. After the colonies formed, the number of CFU was counted. CFUs were normalized to the average CFU of uncoated eTi samples in each of the three replicates ($9.23 \pm 1.06 \times 10^4$, $8.07 \pm 0.90 \times 10^5$, and $4.42 \pm 1.72 \times 10^5$). Each replicate included four samples per group.

2.5.6 LIVE/DEAD fluorescent microscopy—A LIVE/DEAD assay was performed to visualize bacterial viability and biofilm formation on 6 groups of samples (eTi, 0.2Ag, GL/4C, GL/RT, 0.2Ag-GL/4C, and 0.2Ag-GL/RT). The staining solution was prepared by mixing 3 μL of SYTO®9 and 3 μL of propidium iodide in 1 mL of 1×PBS (LIVE/DEAD® BacLight™ Bacterial Viability Kit, Invitrogen, Carlsbad, CA, USA). Micrographs were obtained with a confocal laser scanning microscope (CLSM; FluoView BX2 FV1000, Olympus, Tokyo, Japan) at ×20 magnification (UPLASPO objective, NA=0.85). All CLSM settings were the same across all samples. Fiji-ImageJ (NIH, https://imagej.net/Fiji) was used for micrograph analysis. Three micrographs were taken per sample at arbitrarily selected locations, with each group of three samples.

2.6. *In vitro* cytotoxicity test

2.6.1 Culture of human bone marrow-derived mesenchymal stromal cells (hBMSCs)—hBMSCs were used to evaluate the cytotoxicity of various coatings. hBMSCs were kindly provided by Prof. Jakub Tolar's lab (University of Minnesota, IRB exempt) and maintained in basic fibroblast growth factor (1 ng/mL) and 10% fetal bovine serum supplemented α-minimum essential medium at 37 °C in a 5% CO^2 humidified incubator. The medium was refreshed every third day. Passage 4 cells were used for cytocompatibility assessment of differently coated samples. Cells were passaged and plated on sample surfaces at a density of 10,000 cells/cm^2 in 300 μL medium and cultured for 2 days and 5 days. Cell metabolic activity was assessed at 2 and 5 days in culture and cell morphology was determined at 5 days in culture.

2.6.2 CCK-8 assay—CCK-8 assay (Cell Counting Kit-8, Dojindo, USA) was performed to determine cellular metabolic activity, following the manufacturer's instruction. Briefly, at each time point, medium was replaced with fresh medium containing 10% CCK-8 reagent and cells were incubated for additional 2 h. The reduction of the CCK-8 reagent was quantified colorimetrically by measuring absorbance at 450 nm with a microplate reader

Author Manuscript

Author Manuscript

Author Manuscript

Author Manuscript

(BioTek, Winooski, VT, USA). The absorbance measured for each group was normalized against uncoated eTi.

2.6.3 Immunofluorescence microscopy—At pre-determined time points, immunofluorescence staining against F-actin was performed. Cells were washed with 1× PBS after which they were fixed in 4% paraformaldehyde for 10 min and then permeabilized using 0.25% Triton X-100. Actin filaments were stained using Phalloidin-TRITC (A12381, 1:500, Thermo Fisher Scientific, Waltham, MA, USA) for 1 h and Hoechst 33342 (H3570, 1:1000, Thermo Fisher Scientific) was used to counterstain cell nuclei for 10 min in dark at RT. Samples were washed three times with 1× PBS and imaged with a Leica DM6 B fluorescent microscope (Wetzlar, Germany).

2.7. *In vivo* antimicrobial test

Sprague Dawley male rats at 6 weeks (weight 200±10 g) were obtained from Hunan SJA Laboratory Animal Co., Ltd (Changsha, Hunan, China). The experiment was reviewed and approved by the Ethics Committee of Nanchang University, China (2020-012). Animals were anaesthetized with Ketamine/Xylazine (60:8 mg/kg) intra-peritoneally and given analgesia with Buprenorphine (0.1 mg/kg) subcutaneous injection. The flanks were shaved, and the skin was disinfected with 3% iodine tincture and 75% alcohol. An incision was made parallel to the spine extending to the subdermal fascia. Using an aseptic technique, four groups of sterilized samples (eTi, 0.2Ag, dGL/4C, 0.2Ag-dGL/4C) were inserted into the subcutaneous pocket. Then, 100 μL of 10^8 CFU/mL MRSA bacterial suspension was injected into the subcutaneous pocket around the sample and the wound was sewed up subsequently. The animals were examined 1 h and 2 h post-surgery to ensure recovery from anesthesia and given normal food and water. Rats were sacrificed at the 4th day after implantation of the Ti discs. The Ti discs were carefully removed from each implantation site and separately immersed in 1 mL of PBS for CFU counting and LIVE/DEAD imaging. The tissues surrounding the Ti discs were extracted and fixed in 10% formalin for hematoxylin and eosin (H&E) staining.

2.8. Statistical Analysis

Statistical analysis was performed with SPSS software (version 17.0, SPSS Inc., Chicago, USA). When variances were tested unequal using the Levene's test, that is for the *in vitro* and *in vivo* antimicrobial tests, a one-way ANOVA with Dunnett T3 post hoc test was used to determine statistically significant differences between groups (p-value<0.05). When variances were tested equal using the Levene's test, that is for the WCA and CCK-8 assay tests, a one-way ANOVA with Tuckey post hoc test was used to determine statistically significant differences between groups (p-value<0.05).

3. Results and discussion

3.1 AgNP-GL13K complexes in solution

AgNPs were produced by reduction of silver nitrate. Citrate was used as reductant, complexant, and stabilizer to collectively control size (i.e., 2-4 nm in diameter) and shape (i.e., spherical) of the obtained silver nanocrystallites (Figure 1a).[45] The narrow size

Author Manuscript
Author Manuscript
Author Manuscript
Author Manuscript

distribution assessed by dynamic light scattering (DLS) confirmed the uniformity and stability of AgNPs in both DI water and the pH 9.8 buffer used for production of AgNP-GL13K complexes in solution (Figure 1b). The high negative value of the AgNPs (zeta potential <−55 mV) at alkaline pH provided the necessary electrostatic repulsion between AgNPs to maintain a stable colloidal suspension (Figure 1c).

As previously shown, the self-assembly of GL13K was triggered by the neutralization of the peptide positive charges at pH≥9.6.[34] Here, we further discovered that the peptide incubation temperature influenced the nanostructures and the secondary structures of the self-assembled peptides (Figure 1d-h). When incubated at 4 °C, GL13K formed bundled nanofibrils with a thickness of 10-40 nm and a length as high as a few microns; at room temperature (RT), there were additional 10-50 nm irregular-shaped aggregates formed around the nanofibrils. This indicated that a lower temperature enabled a higher control over the bundled nanofibrils self-assembly process. Though the CD spectra were significantly different at the two temperatures, the secondary structure compositions estimated by the BeStSel method (http://bestsel.elte.hu) revealed a similar percentage of β-sheet (26.9% at 4 °C vs. 26.0% at RT, Figure 1i) and other main secondary structures (Figure S1). Differences in the CD signal were associated with the orientation of the β-sheet structures as antiparallel β-sheets were formed at 4 °C, whereas mostly parallel β-sheets were formed at RT. With significantly lower minimized energies, antiparallel β-sheets are thermodynamically more stable than parallel β-sheets.[46] Thus, GL13K peptides at the lower temperature (i.e., 4 °C) self assembled in a more stable (i.e., antiparallel β-sheets) and more controlled (without aggregates) configuration. The presence of the AgNPs, on the other hand, reduced the overall β-sheet percentage in the GL13K fibrils formed, which was more significant at 4 °C, where a reduction of the antiparallel β-sheets was assessed. These results suggest that the AgNPs might influence the stability of the antimicrobial self-assemblies formed. When GL13K was incubated with AgNPs both at 4 °C and RT, complexes of similar self-assembled nanostructures were formed and decorated with AgNPs (dark areas in the non-stained TEM images, Figure 1f, 1g). The peptide secondary structures (Figure 1h, 1i, Figure S1) were similar to that of GL13K alone at 4°C and RT, respectively. This indicated that the presence of AgNPs in solution did not interfere with the GL13K self-assembly process. In the mixture solutions, electrostatic attraction between the negatively charged AgNPs and the positively charged self-assembled peptides drove the formation of the AgNP-GL13K complexes. It is noted that a large portion of the self-assembled GL13K was not covered by AgNPs, which preserved the strong affinity with the etched Ti surfaces in the following coating process.

3.2 Hybrid nanocoatings on etched titanium

Titanium discs were etched in alkaline solution to activate the surface and increase the surface area to obtain a nanostructured surface topography (Figure S2). The etched Ti (eTi) discs were coated by immersion in solutions with three different compositions: AgNPs, self-assembled GL13K, or AgNP-GL13K complexes. To study the effect of the AgNP/GL13K ratio on the coating, we fixed the GL13K concentration at 1 mg/mL (GL) and varied the AgNP concentrations at 0.2, 1, and 5 mg/mL (0.2Ag, 1Ag, and 5Ag). As the incubation temperature influenced the GL13K self-assembled structures, we also tested eTi

Author Manuscript Author Manuscript Author Manuscript Author Manuscript

after immersion in all coating solutions at either 4 °C or RT (for example, 0.2Ag-GL/4C wherein 0.2 mg/mL AgNP was complexed with 1 mg/mL GL13K at 4 °C).

The surface elemental composition of the coated samples was analyzed by X-ray photoelectron spectroscopy (XPS, Figure 2a, Table 1). The non-coated eTi surfaces showed characteristic Ti2p, C1s, and O1s peaks, which totaled more than 90% of their atomic composition. Additional Na1s was detected on the NaOH-etched control surfaces. The Ag3d peaks were detected in all coatings of AgNPs or AgNP-GL13K hybrid coatings and the N1s peak was detected in all GL13K or AgNP-GL13K coatings, confirming the presence of the antimicrobial nanoparticles and/or peptides, respectively. The relative atomic percentage of Ag was substantially smaller (0.2-2.5%) in coatings with AgNPs than for N (9.1-11.9%) in coatings with GL13K peptides, which is expected as each GL13K molecule contains 18 nitrogen atoms. In other words, the quantity of the Ag atom was comparable to the GL13K molecule in the coatings. The relatively low dose of Ag might reduce the risk of cytotoxicity, which has been the most common limitation for using Ag as an antimicrobial agent.[47] Ag/Ti and N/Ti ratios further revealed that the relative composition of the different coatings was not significantly affected by synthesis conditions for both coatings with only one antimicrobial agent (AgNP or GL13K) and hybrid AgNPs-GL13K coatings. The only exception was the notably higher amount of silver in 5Ag coatings than in 0.2Ag and 1Ag coatings, which was probably due to AgNP aggregation in the solution with the larger concentration of AgNPs. The reduced total surface area of the aggregated AgNPs can be detrimental for their release efficacy and activity, but the close Ag/Ti ratios (0.02-0.04) for all hybrid coatings suggests that the nanoparticles did not aggregate in any of the hybrid coatings (Table 1). Notably, the morphological differences of the self-assembled peptide structures observed at different incubation temperatures did not affect the final composition of GL13K or AgNP-GL13K coatings.

The noncoated eTi surfaces were highly hydrophilic with water contact angle (WCA) <10° as a result of the hydroxyl functionalization from the alkaline etching (Figure 2b). The coatings of AgNPs did not significantly change the hydrophobicity except a small WCA increase in the 5Ag group, which further supported the aggregation of AgNPs in this coating. In comparison, the GL13K or AgNP-GL13K hybrid coatings highly increased the hydrophobicity (WCA = 90-100°), irrespective of the incubation temperature or the AgNP concentration during synthesizing. We have previously described that, as an amphipathic peptide, GL13K self-assembles to supramolecular amphiphiles with the hydrophilic residues physically bonded to the hydrophilic eTi surface and the hydrophobic regions facing toward the solid-liquid interface.[35] Although coatings containing GL13K peptides significantly increase surface hydrophobicity, GL13K-coated implant osteointegration was not negatively affected in a rabbit model.[48]

3.3 *In vitro* antimicrobial activity and cytocompatibility

We first screened the antimicrobial activity of all nanocoatings against the Gram-positive *Streptococcus gordonii*, a primary colonizer of oral surfaces.[49] Using two quantitative methods, i.e., colony forming unit (CFU) counting and ATP assay, we assessed the viability and vitality of bacteria in the biofilms formed on surfaces after 6 h bacterial incubation.

Author Manuscript Author Manuscript Author Manuscript Author Manuscript

All the hybrid AgNP-GL13K coated groups showed remarkably reduced viable bacteria retention compared to the noncoated Ti surface (Figure 3a, 3b). In comparison, the antimicrobial activity of the groups with a single coating (AgNPs or GL13K) was not as effective as the hybrid AgNP-GL13K coating. As the varying AgNP concentrations did not affect the antimicrobial activity, only the lowest Ag concentration (0.2Ag) was used in the following experimentation to minimize potential cytotoxic effects. Among the six selected groups (eTi, 0.2Ag, GL/4C, GL/RT, 0.2Ag-GL/4C, and 0.2Ag-GL/RT) for LIVE/DEAD assays, only the groups with the hybrid AgNP-GL13K coatings showed a large portion of bacteria with compromised membrane (red fluorescence), whereas the other groups had mostly viable bacteria (green fluorescence, Figure S3). This further demonstrated the enhanced antimicrobial efficiency of hybrid versus single-component coatings. The cytocompatibility of the nanocoatings was assessed by directly culturing mesenchymal stromal cells (MSCs) on coated-Ti and control non-coated eTi discs. Cellular responses were determined by assessing cell viability and cell morphology. No significant differences were observed between the differently coated surfaces and the noncoated eTi at both 2 and 5 days in culture (Figure 4a). MSCs exhibited spindle-shaped morphology with well-organized cytoskeletal structures in all groups (Figure 4b). These results indicated that both the hybrid coatings and the single coatings support cell spreading, growth and proliferation to the same extent as noncoated surfaces. Overall, the synthesis temperature (4 °C or RT) did not significantly affect the cytocompatibility of the coatings, but coatings made with peptide solutions at 4°C with the lowest concentration of AgNP showed the statistical significantly highest antimicrobial potency (Figure 3a, 3b). Thus, we performed further antimicrobial experimentation only on coatings prepared at 4 °C.

Biofluid, like oral saliva, flowing over a coating on an implant is persistent, applies continuous shear forces, and supplies sustained nutrition to bacteria. This accelerates bacteria metabolism and biofilm growth.[50] To further test the antimicrobial properties of our hybrid coatings under experimental conditions that recapitulate conditions in the oral environment, we used a drip-flow bioreactor with media flow rates simulating salivary flow on *S. gordonii* biofilms (Figure S4).[51] All samples for each group were placed in an independent channel to avoid contamination from antimicrobial agents released from samples with other coatings. The antimicrobial activity was compared using a LIVE/DEAD assay after 48 h. Generally, the biofilm grew thicker and contained more viable bacteria on the samples placed on the top (Position 1-3) compared to the samples placed on the bottom of each channel (Position 4-6, Figure S5). As biofilms grow differently at the biofilm/air and biofilm/liquid interfaces, we attributed the difference in biofilms grown on different positions of each channel to the fact that the samples in the top positions were fully submerged in medium for all the period of experimentation, whereas the samples located in the lower positions of the channel had areas exposed to air during some stages of the experiment. We thus, limited our analyses, shown in Figure 3c, of comparative effects of the different coatings for samples in Position 2 for each channel, where the biofilm grown was the most robust and homogeneous. Only a small portion of dead bacteria was observed on the antimicrobial coatings with a single antimicrobial component (AgNP or GL13K). In comparison, a large portion of dead bacteria was observed on the hybrid AgNP-GL13K

Author Manuscript

coated surface. Similar trends were also observed in the other positions of the channels (Figure S5).

Two of the most common pathogens associated with orthopedic implant infections, i.e., Gram-positive methicillin resistant *Staphylococcus aureus* (MRSA) and Gram-negative *Pseudomonas aeruginosa*, were used here to assess and extend the potential application of the coatings to orthopedic implants and devices. We also used a D-enantiomer of GL13K (dGL13K) to further enhance the antimicrobial activity of the coatings with either the peptides (dGL/4C) or the AgNP-dGL13K composites (0.2Ag-dGL/4C). It is also noted that D-enantiomer and L-enantiomer of GL13K formed the same self-assembled nanostructures under the same experimental conditions,[34] thus we expected that the synthesis of our hybrid nanocoatings with each of the two enantiomers would not result in differences in the structure of the coatings. dGL13K has been proven to be more active against multiple bacteria strains *in vitro*[52] and *in vivo*[53], including *Enterococcus faecalis*, *S. gordonii, S. aureus,* and *P. aeruginosa*, and present low cytotoxicity, similar to the one for the L-enantiomer[53]. After 6 h incubation in the MRSA solutions, compared to the control eTi group, coatings with a single antimicrobial agent (0.2Ag or dGL/4C) significantly reduced the bacterial burden by only one order of magnitude (Figure 5a). When the Ti surfaces were coated with the AgNP-dGL13K hybrids (0.2Ag-dGL/4C), the bacteria burden was further reduced by two orders of magnitude. All coatings had less antimicrobial potency against *P. aeruginosa* than MRSA, but the AgNP-dGL13K coating was still the most significantly potent surface against this Gram-negative strain (Figure 5b). The different antimicrobial activity against these two bacterial strains might be attributed to the different dGL13K interactions with bacterial cell envelop components.[54] LIVE/DEAD assays further demonstrated the enhanced activity of the hybrid AgNP-dGL13K coatings (Figure 5c and 5d) compared to all other tested groups.

3.4. *In vivo* Subcutaneous Infection Model in Rats

The top performing 0.2Ag-dGL/4C hybrid nanocoating was finally evaluated in a rat subcutaneous infection model over 4 days with an initial MRSA inoculum of 10^7 CFU per implantation site (Figure 6a). The rats were sacrificed at day 4 and the Ti discs were retrieved from the surgical site for counting CFU and LIVE/DEAD imaging. A piece of surrounding tissue was also extracted for histological section to assess peri-implant inflammation. After 4 days, the noncoated eTi samples retained ~10^7 CFU bacteria (Figure 6b). The bacterial attachment on the Ti disc was reduced by one order of magnitude with the single coatings (0.2Ag and dGL/4C) and two orders of magnitude with the hybrid coating of AgNP-dGL13K (0.2Ag-dGL/4C), which paralleled results from the *in vitro* experimentation. More dead bacteria were observed on the discs with the hybrid coatings compared to those with single coatings (Figure 6c), which further supported the killing potency of the hybrid coating. A dense neutrophilic infiltration was observed in the tissues around the noncoated eTi (Figure 6d, Figure S6). A reduction in the inflammatory cell number was obvious in the group with the hybrid AgNP-dGL13K coating. In comparison, the neutrophilic infiltration was still relatively severe in the groups with single coatings. Fibroblasts were also detected in the surrounding tissues of the hybrid nanocoatings, which might be indicative of reduced inflammation (Figure S6). All together, these results support the biocompatibility and *in*

Author Manuscript

Author Manuscript

Author Manuscript

Author Manuscript

vivo antimicrobial activity of the hybrid AgNP-GL13K nanocoatings when implanted in rats. This is a notable outcome that might be associated to the synergistic effects of AMPs and AgNPs and/or their combined bactericidal short- and long-range effects, respectively. Long-term antimicrobial activity, cytotoxicity, tissue integration, and the antimicrobial agent solutions and coating stability need to be further evaluated in future experiments.

4. Conclusions

We developed a hybrid nanocoating on Ti composed of self-assembled AMP nanofibrils decorated with monodispersed AgNPs. The strong hydrophilic interactions between self-assembled AMP amphiphiles and the polar substrates (e.g., Ti) provided a stable antimicrobial coating. The hybrid nanocoating was cytocompatible and increased the antimicrobial efficacy by one and two orders of magnitude compared to single-agent coatings and controls, respectively. The performance of the hybrid nanocoating was preserved *in vivo*, which supports its potential use to reduce post-surgical infections when applied on biomedical implants and devices.

Supplementary Material

Refer to Web version on PubMed Central for supplementary material.

Acknowledgments

This research was supported by the National Institute for Dental and Craniofacial Research of the National Institutes of Health [grant number R01DE026117 to C. A., T90DE0227232 to N.G.F.], the National Institutes of Health's National Center for Advancing Translational Sciences [Translational Research Development Program-TRDP award to Z.Y. from grant UL1TR002494], the National Natural Science Foundation of China [grant number 82160190 to T.S.], the Jiangxi Provincial Department of Science and Technology, China [grant number 20203BBGL73156 to T.S., 20192BBG70022 to T.S.], and 3M Gives [Key Opinion Leaders Scholarship to C.E]. The content is solely the responsibility of the authors and does not necessarily represent the official views of the National Institutes of Health. Parts of this work were carried out in the University of Minnesota I.T. Characterization Facility, which receives partial support from NSF through the MRSEC program. Portions of this work were conducted in the Minnesota Nano Center, which is supported by the Narional Science Foundation through the National Coordinated (NNCI) under Award Number ECCS-2025124. Confocal laser scanning microscopy was performed at the University of Minnesota – University Imaging Center (SCR_020997).

REFERENCES

[1]. Arciola CR, Campoccia D, Montanaro L, Implant infections: Adhesion, biofilm formation and immune evasion, Nat. Rev. Microbiol 16 (2018) 397–409. doi: 10.1038/s41579-018-0019-y. [PubMed: 29720707]

[2]. Pye AD, Lockhart DEA, Dawson MP, Murray CA, Smith AJ, A review of dental implants and infection, J. Hosp. Infect 72 (2009) 104–110. doi: 10.1016/j.jhin.2009.02.010. [PubMed: 19329223]

[3]. Filipović U, Dahmane RG, Ghannouchi S, Zore A, Bohinc K, Bacterial adhesion on orthopedic implants, Adv. Colloid Interface Sci (2020). doi:10.1016/j.cis.2020.102228.

[4]. Zimmerli W, Clinical presentation and treatment of orthopaedic implant-associated infection, J. Intern. Med 276 (2014) 111–119. doi:10.1111/joim.12233. [PubMed: 24605880]

[5]. B. HJ, van der MHC, Guruprakash S, J. PC, van den DJJAM, Z. SAJ, S. MJ, G. DW, Biomaterial-Associated Infection: Locating the Finish Line in the Race for the Surface, Sci. Transl. Med 4 (2012) 153rv10–153rv10. doi:10.1126/scitranslmed.3004528.

Author Manuscript Author Manuscript Author Manuscript Author Manuscript

[6]. Li B, Webster TJ, Bacteria antibiotic resistance: New challenges and opportunities for implant-associated orthopedic infections, J. Orthop. Res 36 (2018) 22–32. doi:10.1002/jor.23656. [PubMed: 28722231]

[7]. Chouirfa H, Bouloussa H, Migonney V, Falentin-Daudré C, Review of titanium surface modification techniques and coatings for antibacterial applications, Acta Biomater. 83 (2019) 37–54. doi:10.1016/j.actbio.2018.10.036. [PubMed: 30541702]

[8]. Zhao L, Chu PK, Zhang Y, Wu Z, Antibacterial coatings on titanium implants, J. Biomed. Mater. Res. - Part B Appl. Biomater 91 (2009) 470–480. doi:10.1002/jbm.b.31463.

[9]. Mutreja I, Ye Z, Aparicio C, Cell responses to titanium and titanium alloys, in: M.B.T.- H. of Mozafari BB (Ed.), Handb. Biomater. Biocompat, Woodhead Publishing, 2020: pp. 423–452. doi:10.1016/b978-0-08-102967-1.00020-7.

[10]. Jin G, Cao H, Qiao Y, Meng F, Zhu H, Liu X, Osteogenic activity and antibacterial effect of zinc ion implanted titanium, Colloids Surfaces B Biointerfaces. (2014). doi: 10.1016/j.colsurfb.2014.02.025.

[11]. Wan YZ, Xiong GY, Liang H, Raman S, He F, Huang Y, Modification of medical metals by ion implantation of copper, Appl. Surf. Sci 253 (2007) 9426–9429. doi: 10.1016/j.apsusc.2007.06.031.

[12]. Elizabeth E, Baranwal G, Krishnan AG, Menon D, Nair M, ZnO nanoparticle incorporated nanostructured metallic titanium for increased mesenchymal stem cell response and antibacterial activity, Nanotechnology. 25 (2014). doi:10.1088/0957-4484/25/11/115101.

[13]. Stigter M, Bezemer J, De Groot K, Layrolle P, Incorporation of different antibiotics into carbonated hydroxyapatite coatings on titanium implants, release and antibiotic efficacy, J. Control. Release 99 (2004) 127–137. doi:10.1016/j.jconrel.2004.06.011. [PubMed: 15342186]

[14]. Alt V, Bitschnau A, Österling J, Sewing A, Meyer C, Kraus R, Meissner SA, Wenisch S, Domann E, Schnettler R, The effects of combined gentamicin-hydroxyapatite coating for cementless joint prostheses on the reduction of infection rates in a rabbit infection prophylaxis model, Biomaterials. 27 (2006) 4627–4634. doi: 10.1016/j.biomaterials.2006.04.035. [PubMed: 16712926]

[15]. Kazemzadeh-Narbat M, Lai BFL, Ding C, Kizhakkedathu JN, Hancock REW, Wang R, Multilayered coating on titanium for controlled release of antimicrobial peptides for the prevention of implant-associated infections, Biomaterials. 34 (2013) 5969–5977. doi: 10.1016/j.biomaterials.2013.04.036. [PubMed: 23680363]

[16]. Chen R, Willcox MDP, Ho KKK, Smyth D, Kumar N, Antimicrobial peptide melimine coating for titanium and its in vivo antibacterial activity in rodent subcutaneous infection models, Biomaterials. 85 (2016) 142–151. doi: 10.1016/j.biomaterials.2016.01.063. [PubMed: 26871890]

[17]. Yazici H, O'Neill MB, Kacar T, Wilson BR, Oren EE, Sarikaya M, Tamerler C, Engineered Chimeric Peptides as Antimicrobial Surface Coating Agents toward Infection-Free Implants, ACS Appl. Mater. Interfaces 8 (2016) 5070–5081. doi:10.1021/acsami.5b03697. [PubMed: 26795060]

[18]. Wang L, Erasquin UJ, Zhao M, Ren L, Zhang MY, Cheng GJ, Wang Y, Cai C, Stability, antimicrobial activity, and cytotoxicity of poly(amidoamine) dendrimers on titanium substrates, ACS Appl. Mater. Interfaces 3 (2011) 2885–2894. doi:10.1021/am2004398. [PubMed: 21774463]

[19]. Liu L, Peng W, Zhang X, Peng J, Liu P, Shen J, Rational design of phosphonate/quaternary amine block polymer as an high-efficiency antibacterial coating for metallic substrates, J. Mater. Sci. Technol 62 (2021) 96–106. doi:10.1016/j.jmst.2020.05.060.

[20]. Croes M, Bakhshandeh S, van Hengel IAJ, Lietaert K, van Kessel KPM, Pouran B, van der Wal BCH, Vogely HC, Van Hecke W, Fluit AC, Boel CHE, Alblas J, Zadpoor AA, Weinans H, Amin Yavari S, Antibacterial and immunogenic behavior of silver coatings on additively manufactured porous titanium, Acta Biomater. 81 (2018) 315–327. doi: 10.1016/j.actbio.2018.09.051. [PubMed: 30268917]

[21]. Zhou W, Jia Z, Xiong P, Yan J, Li Y, Li M, Cheng Y, Zheng Y, Bioinspired and Biomimetic AgNPs/Gentamicin-Embedded Silk Fibroin Coatings for Robust Antibacterial and Osteogenetic Applications, ACS Appl. Mater. Interfaces 9 (2017) 25830–25846. doi:10.1021/acsami.7b06757. [PubMed: 28731325]

Author Manuscript

Author Manuscript

Author Manuscript

Author Manuscript

[22]. Zhou W, Yan J, Li Y, Wang L, Jing L, Li M, Yu S, Cheng Y, Zheng Y, Based on the synergistic effect of Mg2+and antibacterial peptides to improve the corrosion resistance, antibacterial ability and osteogenic activity of magnesium-based degradable metals, Biomater. Sci 9 (2021) 807–825. doi:10.1039/d0bm01584a. [PubMed: 33210105]

[23]. Xie X, Mao C, Liu X, Zhang Y, Cui Z, Yang X, Yeung KWK, Pan H, Chu PK, Wu S, Synergistic Bacteria Killing through Photodynamic and Physical Actions of Graphene Oxide/Ag/Collagen Coating, ACS Appl. Mater. Interfaces 9 (2017) 26417–26428. doi: 10.1021/acsami.7b06702. [PubMed: 28715631]

[24]. Tan L, Li J, Liu X, Cui Z, Yang X, Zhu S, Li Z, Yuan X, Zheng Y, Yeung KWK, Pan H, Wang X, Wu S, Rapid Biofilm Eradication on Bone Implants Using Red Phosphorus and Near-Infrared Light, Adv. Mater 30 (2018). doi: 10.1002/adma.201801808.

[25]. Li Y, Yang Y, Qing Y, Li R, Tang X, Guo D, Qin Y, Enhancing zno-np antibacterial and osteogenesis properties in orthopedic applications: A review, Int. J. Nanomedicine 15 (2020) 6247–6262. doi:10.2147/IJN.S262876. [PubMed: 32903812]

[26]. Jin G, Qin H, Cao H, Qian S, Zhao Y, Peng X, Zhang X, Liu X, Chu PK, Synergistic effects of dual Zn/Ag ion implantation in osteogenic activity and antibacterial ability of titanium, Biomaterials. 35 (2014) 7699–7713. doi: 10.1016/j.biomaterials.2014.05.074. [PubMed: 24947228]

[27]. Xia C, Cai D, Tan J, Li K, Qiao Y, Liu X, Synergistic Effects of N/Cu Dual Ions Implantation on Stimulating Antibacterial Ability and Angiogenic Activity of Titanium, ACS Biomater. Sci. Eng 4 (2018) 3185–3193. doi:10.1021/acsbiomaterials.8b00501. [PubMed: 33435059]

[28]. Zhou J, Zhao L, Multifunction Sr, Co and F co-doped microporous coating on titanium of antibacterial, angiogenic and osteogenic activities, Sci. Rep 6 (2016). doi: 10.1038/srep29069.

[29]. Yu Y, Jin G, Xue Y, Wang D, Liu X, Sun J, Multifunctions of dual Zn/Mg ion co-implanted titanium on osteogenesis, angiogenesis and bacteria inhibition for dental implants, Acta Biomater. 49 (2017) 590–603. doi:10.1016/j.actbio.2016.11.067. [PubMed: 27915020]

[30]. Pal I, Bhattacharyya D, Kar RK, Zarena D, Bhunia A, Atreya HS, A Peptide-Nanoparticle System with Improved Efficacy against Multidrug Resistant Bacteria, Sci. Rep 9 (2019). doi:10.1038/s41598-019-41005-7.

[31]. Ruden S, Hilpert K, Berditsch M, Wadhwani P, Ulrich AS, Synergistic interaction between silver nanoparticles and membrane-permeabilizing antimicrobial peptides, Antimicrob. Agents Chemother 53 (2009) 3538–3540. doi: 10.1128/AAC.01106-08. [PubMed: 19528287]

[32]. Gao J, Na H, Zhong R, Yuan M, Guo J, Zhao L, Wang Y, Wang L, Zhang F, One step synthesis of antimicrobial peptide protected silver nanoparticles: The core-shell mutual enhancement of antibacterial activity, Colloids Surfaces B Biointerfaces. 186 (2020). doi: 10.1016/j.colsurfb.2019.110704.

[33]. Pal I, Brahmkhatri VP, Bera S, Bhattacharyya D, Quirishi Y, Bhunia A, Atreya HS, Enhanced stability and activity of an antimicrobial peptide in conjugation with silver nanoparticle, J. Colloid Interface Sci 483 (2016) 385–393. doi: 10.1016/j.jcis.2016.08.043. [PubMed: 27585423]

[34]. Ye Z, Zhu X, Acosta S, Kumar D, Sang T, Aparicio C, Self-assembly dynamics and antimicrobial activity of all l- and d-amino acid enantiomers of a designer peptide, Nanoscale. 11 (2019)266–275. doi:10.1039/c8nr07334a.

[35]. Ye Z, Kobe AC, Sang T, Aparicio C, Unraveling dominant surface physicochemistry to build antimicrobial peptide coatings with supramolecular amphiphiles, Nanoscale. 12 (2020) 20767–20775. doi:10.1039/d0nr04526h. [PubMed: 33030163]

[36]. Ye Z, Aparicio C, Modulation of supramolecular self-assembly of an antimicrobial designer peptide by single amino acid substitution: implications on peptide activity, Nanoscale Adv. 1 (2019) 4679–4682. doi:10.1039/c9na00498j. [PubMed: 31844837]

[37]. Moussa DG, Kirihara JA, Ye Z, Fischer NG, Khot J, Witthuhn BA, Aparicio C, Dentin Priming with Amphipathic Antimicrobial Peptides, J. Dent. Res 98 (2019) 1112–1121. doi: 10.1177/0022034519863772. [PubMed: 31313946]

[38]. Boda SK, Fischer NG, Ye Z, Aparicio C, Dual Oral Tissue Adhesive Nanofiber Membranes for pH-Responsive Delivery of Antimicrobial Peptides, Biomacromolecules. 21 (2020) 4945–4961. doi:10.1021/acs.biomac.0c01163. [PubMed: 32961056]

Author Manuscript Author Manuscript Author Manuscript Author Manuscript

[39]. Ye Z, Zhu X, Mutreja I, Boda SK, Fischer NG, Zhang A, Lui C, Qi Y, Aparicio C, Biomimetic mineralized hybrid scaffolds with antimicrobial peptides, Bioact. Mater 6 (2021) 2250–2260. doi:10.1016/j.bioactmat.2020.12.029. [PubMed: 33553813]

[40]. Chen X, Flirt H, Li Y, Gorr SU, Aparicio C, Antimicrobial GL13K peptide coatings killed and ruptured the wall of streptococcus gordonii and prevented formation and growth of biofilms, PLoS One. 9 (2014). doi:10.1371/journal.pone.0111579.

[41]. Holmberg KV, Abdolhosseini M, Li Y, Chen X, Gorr SU, Aparicio C, Bio-inspired stable antimicrobial peptide coatings for dental applications, Acta Biomater. 9 (2013) 8224–8231. doi: 10.1016/j.actbio.2013.06.017. [PubMed: 23791670]

[42]. Pillai ZS, Kamat PV, What factors control the size and shape of silver nanoparticles in the citrate ion reduction method?, J. Phys. Chem. B (2004). doi:10.1021/jp037018r.

[43]. Alkilany AM, Abulateefeh SR, Mills KK, Bani Yaseen AI, Hamaly MA, Alkhatib HS, Aiedeh KM, Stone JW, Colloidal stability of citrate and mercaptoacetic acid capped gold nanoparticles upon lyophilization: Effect of capping ligand attachment and type of cryoprotectants, Langmuir. 30 (2014) 13799–13808. doi:10.1021/la504000v. [PubMed: 25356538]

[44]. Micsonai A, Wien F, Kernya L, Lee Y-H, Goto Y, Réfrégiers M, Kardos J, Accurate secondary structure prediction and fold recognition for circular dichroism spectroscopy, Proc. Natl. Acad. Sci 112 (2015) E3095 LP–E3103. doi:10.1073/pnas.1500851112. [PubMed: 26038575]

[45]. Pillai ZS, Kamat PV, What factors control the size and shape of silver nanoparticles in the citrate ion reduction method?, J. Phys. Chem. B 108 (2004) 945–951. doi:10.1021/jp037018r.

[46]. Chou KC, Pottle M, Némethy G, Ueda yuzo, Scheraga HA, Structure of β-sheets. Origin of the right-handed twist and of the increased stability of antiparallel over parallel sheets, J. Mol. Biol (1982). doi:10.1016/0022-2836(82)90163-2.

[47]. Akter M, Sikder MT, Rahman MM, Ullah AKMA, Hossain KFB, Banik S, Hosokawa T, Saito T, Kurasaki M, A systematic review on silver nanoparticles-induced cytotoxicity: Physicochemical properties and perspectives, J. Adv. Res 9 (2018) 1–16. doi: 10.1016/j.jare.2017.10.008. [PubMed: 30046482]

[48]. Chen X, Zhou XC, Liu S, Wu RF, Aparicio C, Wu JY, In vivo osseointegration of dental implants with an antimicrobial peptide coating, J. Mater. Sci. Mater. Med 28 (2017) 76. doi: 10.1007/s10856-017-5885-8. [PubMed: 28386851]

[49]. Rath H, Feng D, Neuweiler I, Stumpp NS, Nackenhorst U, Stiesch M, Biofilm formation by the oral pioneer colonizer Streptococcus gordonii: An experimental and numerical study, FEMS Microbiol. Ecol 93 (2017). doi:10.1093/femsec/fix010.

[50]. Sawant SN, Selvaraj V, Prabhawathi V, Doble M, Antibiofilm Properties of Silver and Gold Incorporated PU, PCLm, PC and PMMA Nanocomposites under Two Shear Conditions, PLoS One. 8 (2013). doi:10.1371/journal.pone.0063311.

[51]. Fenoll-Palomares C, Muñoz-Montagud JV, Sanchiz V, Herreros B, Hernández V, Mínguez M, Benages A, Débito basal, pH y capacidad tampón de la secrecion salivar en sujetos sanos, Rev. Esp. Enfermedades Dig 96 (2004) 773–783. doi: 10.4321/S1130-01082004001100005.

[52]. Hirt H, Hall JW, Larson E, Gorr SU, A D-enantiomer of the antimicrobial peptide GL13K evades antimicrobial resistance in the Gram positive bacteria Enterococcus faecalis and Streptococcus gordonii, PLoS One. 13 (2018). doi: 10.1371/journal.pone.0194900.

[53]. Gorr SU, Flory CM, Schumacher RJ, In vivo activity and low toxicity of the second-generation antimicrobial peptide DGL13K, PLoS One. 14 (2019). doi:10.1371/journal.pone.0216669.

[54]. Ye Z, Aparicio C, Interactions of two enantiomers of a designer antimicrobial peptide with structural components of the bacterial cell envelope, J. Pept. Sci (2021). doi: 10.1002/psc.3299.

Author Manuscript Author Manuscript Author Manuscript Author Manuscript

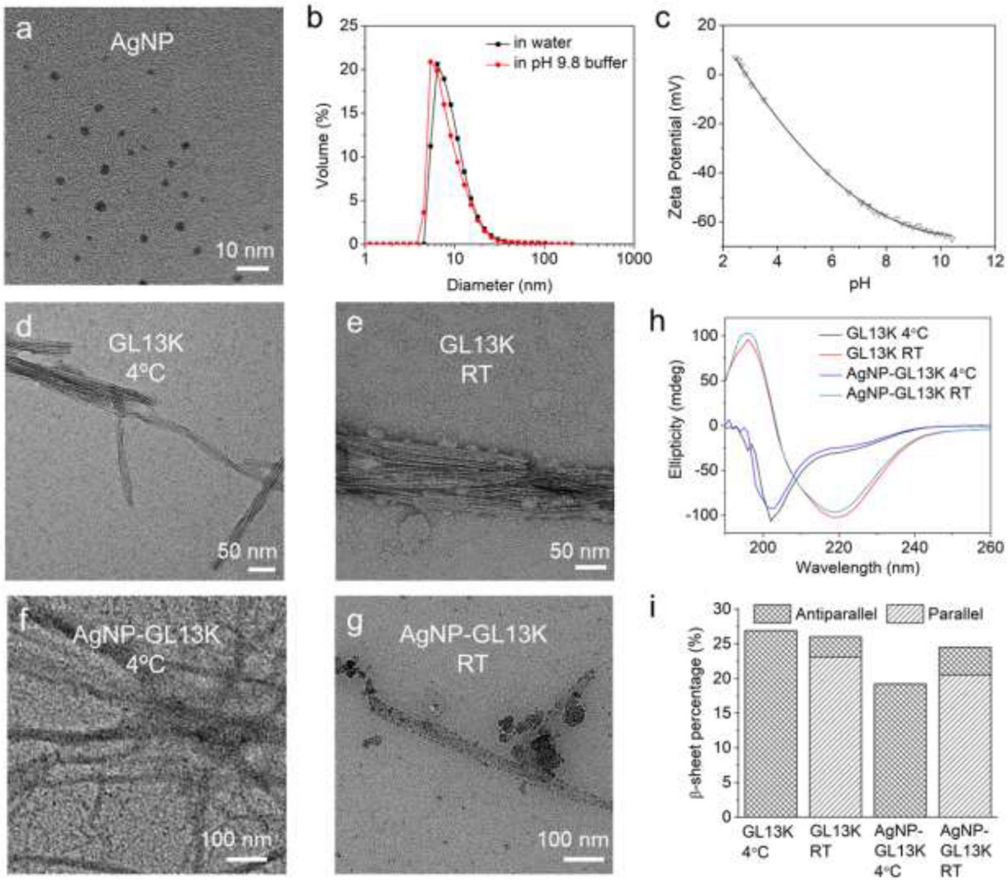

Figure 1. Characterization of antimicrobial inorganic and peptidic nanostructures as well as their complexes in coating solutions.

(a) A representative TEM micrograph of 1 mg/mL AgNPs in DI water. (b) Volume distribution of 0.2 mg/mL AgNPs in DI water and in the pH 9.8 borax-NaOH buffer that was used to prepare the coating solution. (c) Titration of AgNPs zeta potential. Negative-stained TEM micrographs of GL13K (d) self-assembled nanofibrils at 4 °C or (e) self-assembled nanofibrils and aggregated nanospheres at RT. TEM micrographs of non-stained AgNP-GL13K complex at (f) 4 °C or (g) RT. Dark areas in (f, g) are AgNPs decorating GL13K self-assembled nanofibrils and/or aggregated nanospheres. (h) CD spectra of 1 mg/mL GL13K and AgNP-GL13K complex at 4 °C and RT. (i) Estimated percentages of antiparallel and parallel β-sheet secondary structure in GL13K and AgNP-GL13K complex at 4 °C and RT.

Author Manuscript

Author Manuscript

Author Manuscript

Author Manuscript

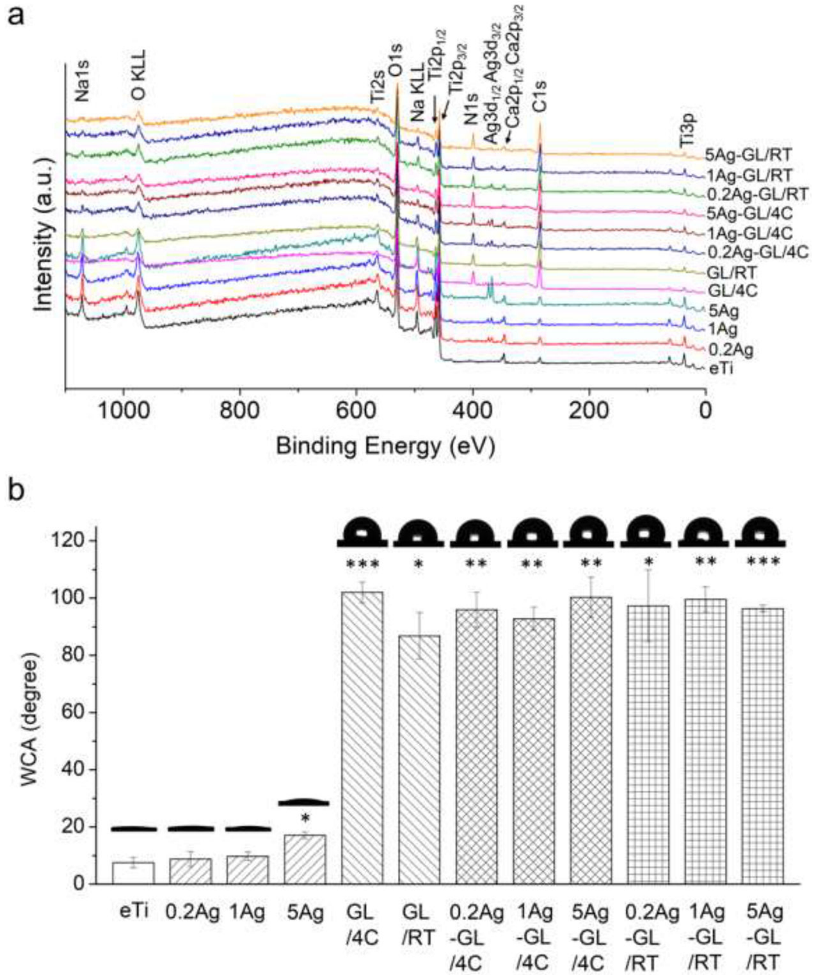

Figure 2. Physical-chemical surface characterization of the hybrid antimicrobial nanocoatings.

(a) Representative XPS spectra and (b) WCA (average ± standard deviation, N=3) and representative photomicrographs for the 12 tested groups: noncoated eTi and eTi coated with AgNP (varied concentration; 0.2Ag, 1Ag, and 5Ag), GL13K (varied temperature; GL/4C and GL/RT), or hybrid AgNP+GL13K (varied concentration and temperature; 0.2Ag-GL/4C, 1Ag-GL/4C, 5Ag-GL/4C, 0.2Ag-GL/RT, 1Ag-GL/RT, and 5Ag-GL/RT). Asterisks indicate statistically significant differences vs. noncoated eTi control surfaces: * $p\text{-value}<0.05$; ** $p\text{-value}<0.01$; *** $p\text{-value}<0.001$.

Author Manuscript

Author Manuscript

Author Manuscript

Author Manuscript

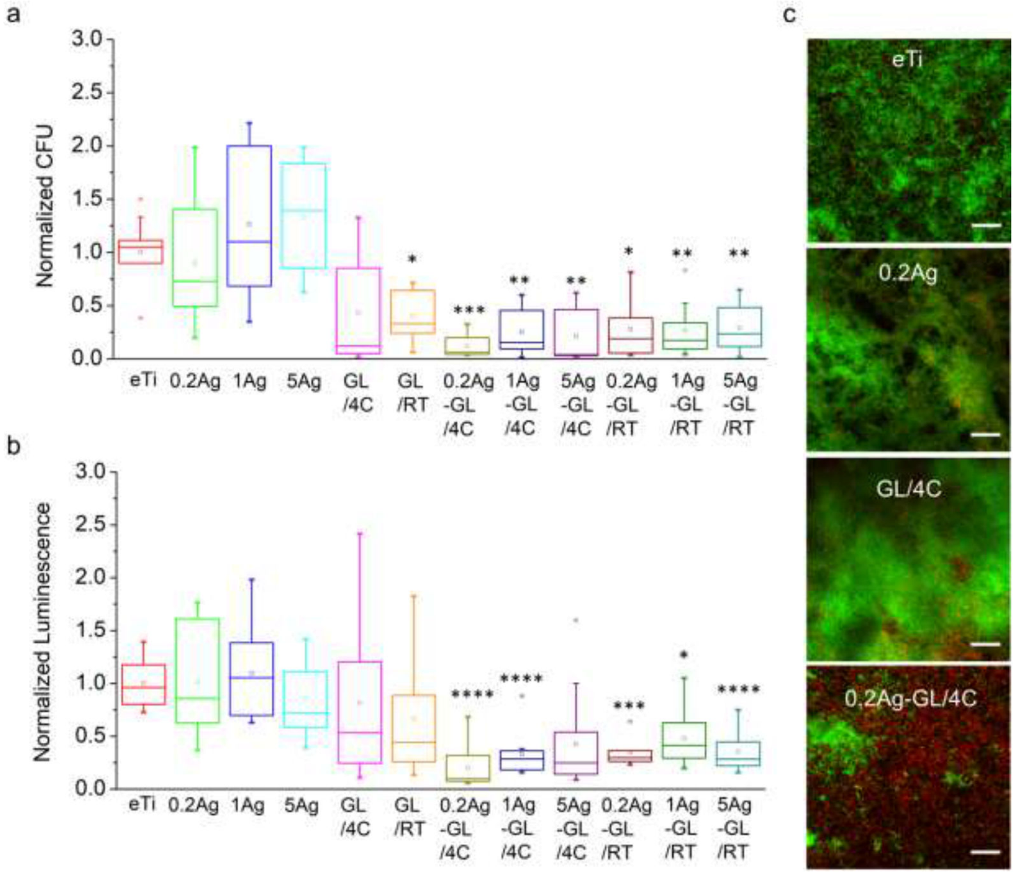

Figure 3. ***In vitro*** **antimicrobial activity of the hybrid nanocoatings against** ***S. gordonii*****.**

(a) CFU and (b) ATP luminescence intensity normalized to uncoated eTi control of *S. gordonii* that colonized the tested surfaces after 6 h incubation in quasi-static conditions. Asterisks indicate statistically significant differences vs. uncoated eTi control surfaces: * p-value<0.05; ** p-value<0.01; *** p-value<0.001; **** p-value<0.0001. Three biological replicates were performed. (c) Representative CLSM images of LIVE/DEAD stained *S. gordonii* biofilms on the tested surfaces after 48 h incubation in a drip-flow bioreactor. Four representative groups (eTi, 0.2Ag, GL/4C, and 0.2Ag-GL/4C) were tested in independent channels of our custom-made 4-channel bioreactor. All scale bars are 50 μm.

Author Manuscript
Author Manuscript
Author Manuscript
Author Manuscript

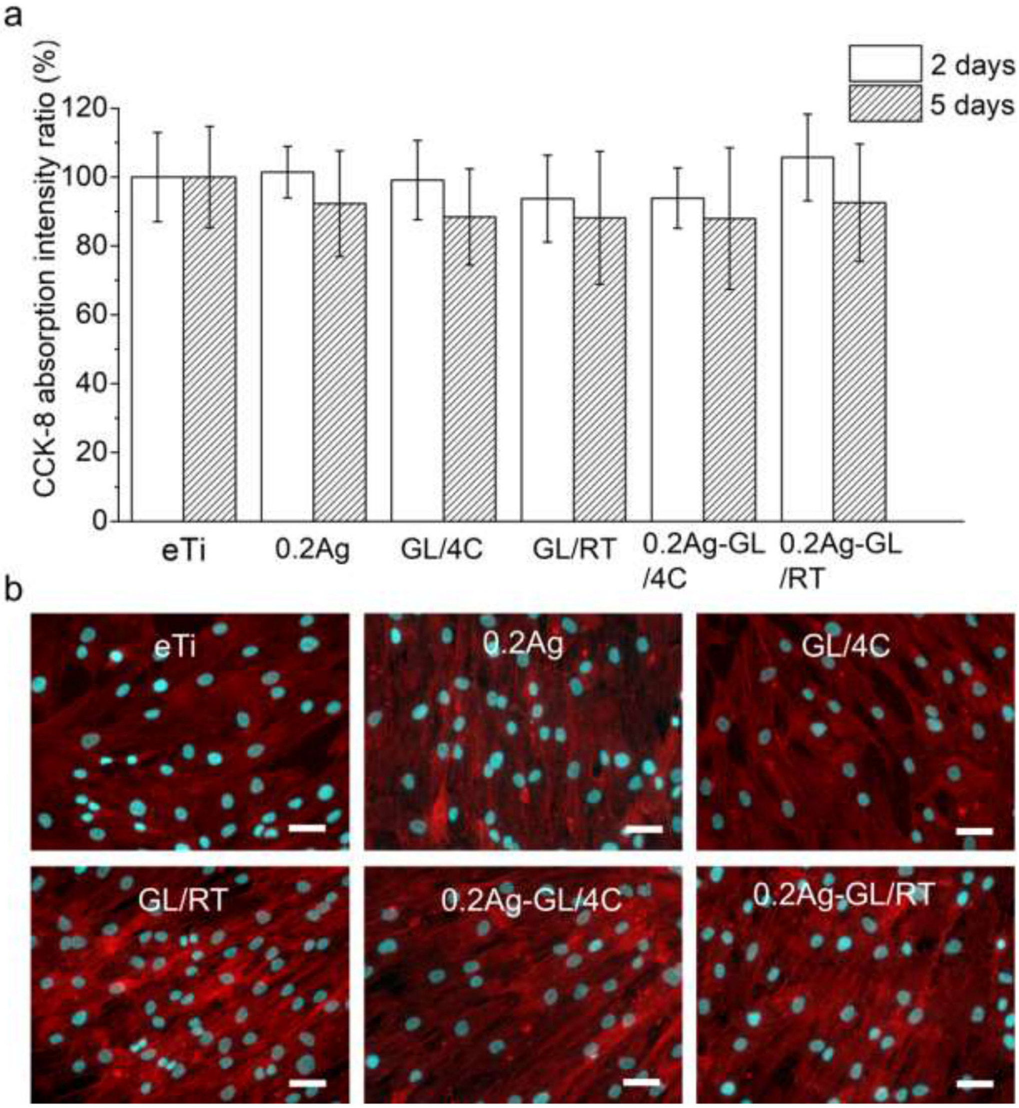

Figure 4. *In vitro* cytocompatibility of the hybrid antimicrobial nanocoatings.

(a) Proliferation of hBMSC (CCK-8 assay) normalized against uncoated eTi control on tested surfaces after 2 d and 5 d in culture. No statistically significant differences were found between different groups; p-value<0.05. Two biological replicates were performed with four samples for each group in each experiment (N=8). (b) Cell morphology visualized by immunofluorescence (F-actin – red and nuclei – cyan) staining after 5 d in culture. All scale bars are 50 μm.

Author Manuscript
Author Manuscript
Author Manuscript
Author Manuscript

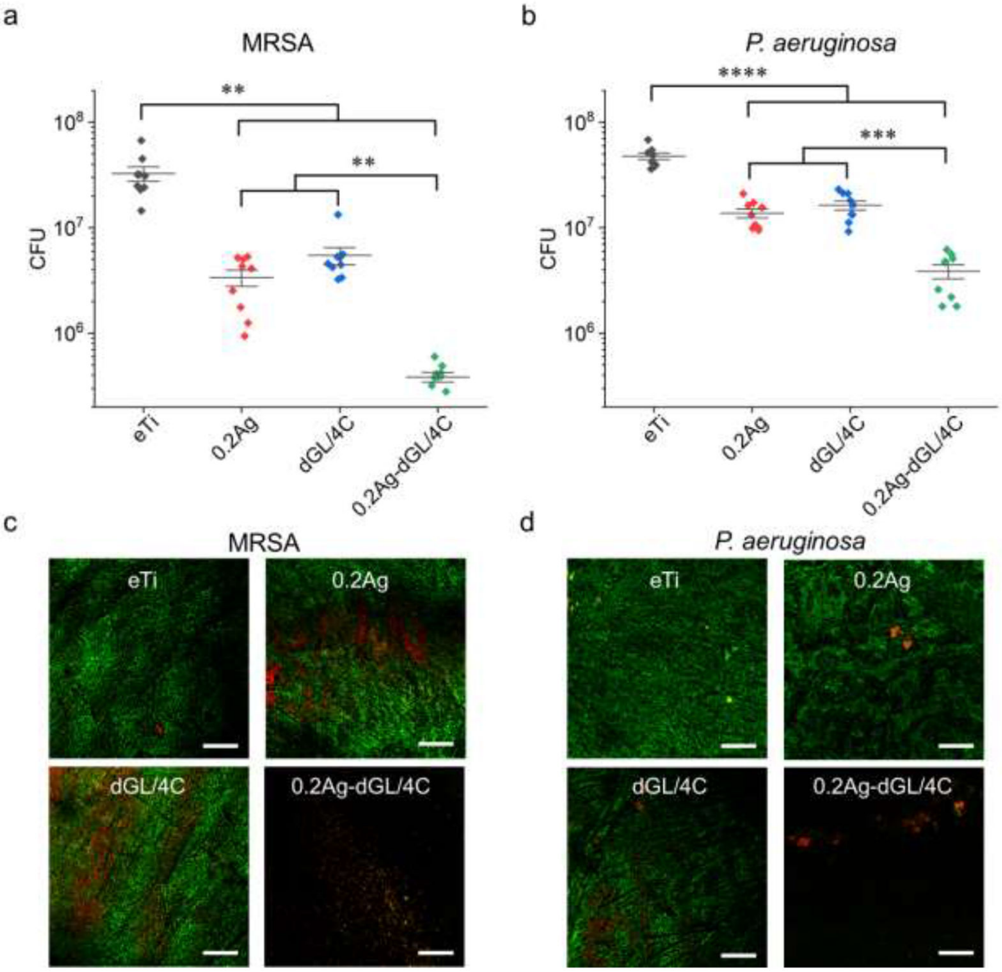

Figure 5. *In vitro* antimicrobial activity of the hybrid nanocoatings against MRSA and *P. aeruginosa*.

(a, b) CFU and (c. d) representative LIVE/DEAD stain CLSM images of (a, c) MRSA or (b, d) *P. aeruginosa* biofilms grown on the tested surfaces after 6 h incubation in quasi-static conditions. Asterisks indicate statistically significant differences between connected groups: * p-value<0.05; ** p-value<0.01; *** p-value<0.001; **** p-value<0.0001. Three biological replicates with three samples in each experiment for each group were performed for each bacteria strain (N=9). All scale bars are 100 μm.

Author Manuscript
Author Manuscript
Author Manuscript
Author Manuscript

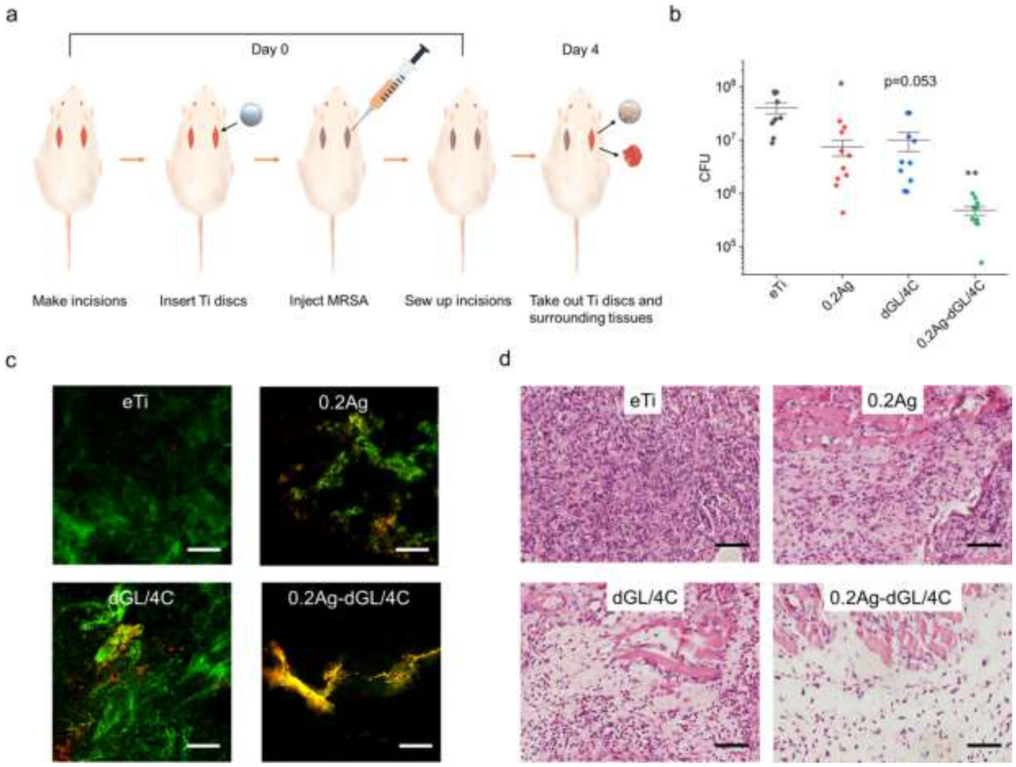

Figure 6. *In vivo* antimicrobial activity of the hybrid nanocoatings against MRSA.

(a) Schematics of the *in vivo* experimental design. At Day 0, eTi control and antimicrobial coated discs were implanted in open incisions and infected by injection with MRSA. After 4 days, the discs and surrounding tissues were removed for analysis. (b) CFU (N=10 for each group) and (c) representative LIVE/DEAD stain CLSM images of MRSA that colonized and were collected from implanted discs. (d) Optical microscopy images of tissues surrounded the infected discs (H&E stain). Asterisks indicate statistically significant differences vs uncoated eTi control discs: * p-value<0.05; ** p-value<0.01. All scale bars are 100 μm.

Author Manuscript

Author Manuscript

Author Manuscript

Author Manuscript

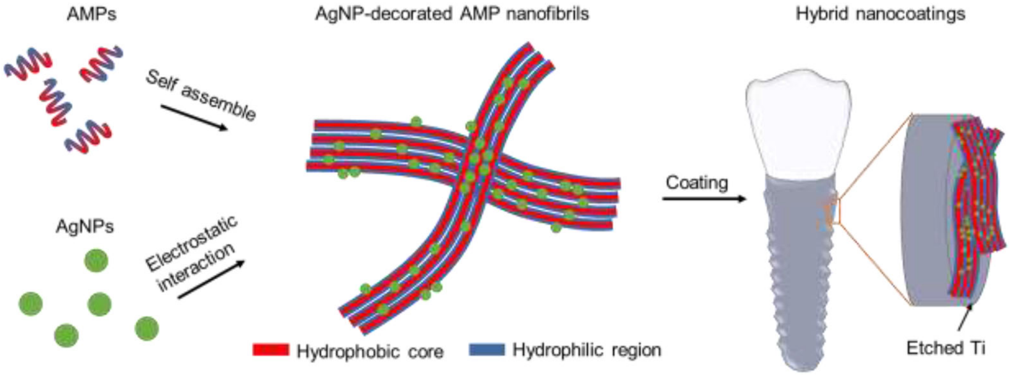

Scheme 1.

Schematics of the syntheses of the AMP/AgNP nanocomposites and the hybrid nanocoatings on etched Ti.

Author Manuscript Author Manuscript Author Manuscript Author Manuscript

Table 1.

XPS elemental composition (atomic %, mean ± standard deviation, N=3) for noncoated eTi control and AgNPs and/or GL13K coated surfaces.

Group	C1s	N1s	O1s	Ti2p	Ag3d	Others (Na1s, Ca2p)	N:Ti	Ag:Ti
eTi	10.42±1.43	0.42±0.42	60.44±1.37	19.94±0.56	0.03±0.05	8.75±0.42	0.02	0.00
0.2Ag	12.36±0.87	0.49±0.65	61.45±2.39	16.21±1.08	0.42±0.05	9.08±1.85	0.03	0.03
1Ag	11.81±1.25	0.63±0.48	59.97±1.43	17.61±0.89	0.53±0.33	9.45±1.03	0.04	0.03
5Ag	13.97±0.89	0.57±0.58	60.08±1.31	14.94±0.97	2.17±0.64	8.28±1.47	0.04	0.15
GL/4C	48.56±2.99	11.94±1.49	28.69±2.17	6.01±1.00	0.05±0.04	4.76±2.04	1.99	0.01
GL/RT	40.56±2.25	9.28±0.84	36.40±1.81	8.30±1.28	0.03±0.03	5.44±1.26	1.12	0.00
0.2Ag-GL/4C	38.87±1.44	9.11±0.78	40.33±1.09	9.10±0.55	0.24±0.13	2.35±0.40	1.00	0.03
1Ag-GL/4C	41.58±4.33	9.41±1.37	37.18±3.41	8.70±1.56	0.29±0.16	2.84±0.90	1.08	0.03
5Ag-GL/4C	41.27±2.47	10.10±0.94	38.03±2.11	8.33±1.01	0.19±0.08	2.08±0.89	1.21	0.02
0.2Ag-GL/RT	37.83±2.19	9.44±1.02	40.20±1.92	8.91±0.72	0.34±0.30	3.28±0.99	1.06	0.04
1Ag-GL/RT	41.35±4.14	10.15±1.37	37.02±3.28	8.01±1.39	0.18±0.15	3.29±0.78	1.27	0.02
5Ag-GL/RT	43.23±3.87	10.38±1.01	36.01±2.50	7.60±1.49	0.27±0.13	2.51±0.84	1.37	0.04